614 | https://doi.org/10.3311/PPci.19777
Creative Commons Attribution

Periodica Polytechnica Civil Engineering, 66(2), pp. 614–626, 2022

Seismic Performance and Reliability Evaluation of Ductile RC Frame Structures with Infills

Jianchen Zhao[1], Hongxing Qiu[1*]

[1] Key Laboratory of Concrete and Prestressed Concrete Structures of the Ministry of Education, Southeast University, No. 90 Chengxian Street, 210096 Nanjing, Xuanwu, China
[*] Corresponding author, e-mail: qiuhx@seu.edu.cn

Received: 30 December 2021, Accepted: 09 March 2021, Published online: 17 March 2022

Abstract

Ductile RC frames are often considered to have superior seismic performance even with infills. However, the seismic performance of this type of structure needs to be reassessed considering the additional shear requirements produced by the infills-column interaction and the increased seismic hazard due to the impact of infills on the vibration period of the structure. This paper presents a performance-based earthquake engineering framework aimed at the assessment of the comprehensive seismic performance of ductile RC frames with infills. A series of common configurations are considered in the analysis: bare frame (BF), upper-infilled frame (UIF), all-infilled frame (AIF), and corresponding stirrup-reduction frames with both infills-induced shear failure behavior of column and influence of structural vibration period considered. The results show that infills changed the failure modes and dynamic characteristics of ductile structures and shear failure occurs in all-infilled frame columns. Even though the all-infilled frame meets the shear requirement, its collapse probability is higher than the bare frame due to the high seismic hazard caused by a shorter vibration period.

Keywords

infilled RC frame, shear failure, Incremental Dynamic Analysis, reliability assessment

1 Introduction

The frame-constrained infills may have a positive effect on the seismic performance of the structure: improving the lateral resistance of the frame and increasing the energy dissipation capacity of the structure [1]. On the other hand, the existence of infills may cause potential negative effects, such as the torsion effect caused by irregular distribution of floor stiffness [2] and the soft-story mechanism caused by vertical irregularity [3]. It is also found that the interaction between infills and frames increases the risk of shear failure on the column in the post-earthquake observation, which leads to severe structural damage and collapse [4, 5].

Many studies have been proposed on the behavior of infilled frame experimentally and theoretically [6–7]. Reasonable finite element models have also been proposed, including micro refined model [8] and macro model. It has been shown that the sophisticated micro model should be used when local failure modes of masonry blocks are tended to investigated [9]. The macro model represented by equivalent structs has also been widely developed. Particularly, multi-strut method [10] provides more realistic estimations of the internal shear force in column which is competitive for studying local interactions between infills and columns. By introducing nonlinear constitutive conditions, the simplified model can represent the proximate response of global structure, hence can be easily used in dynamic analysis of large structures. In addition, the influence of out-of-plane deformation has also been studied [11], because it can affect the in-plane behavior of infills. The numerical models considering out-of-plane response was also proposed and applied [12, 13].

Although many studies focus on the interaction between infills and frames, case studies of global structures are still inadequate. Uva et al. [14] took an existing non-ductile reinforced concrete frame building as a case to perform nonlinear static analyses. The results showed that the infills-frame interaction near the structural joint had a significant impact on the global response of the structure.

Celarec and Dolšek [15] developed an iteration-based push-over analysis program aimed at capturing the shear failure of columns. Burton and Deierlein [16] investigated the seismic performance of non-ductile RC frames through incremental dynamic analysis to disclose the drawbacks

Cite this article as: Zhao, J., Qiu, H. "Seismic Performance and Reliability Evaluation of Ductile RC Frame Structures with Infills", Periodica Polytechnica Civil Engineering, 66(2), pp. 614–626, 2022. https://doi.org/10.3311/PPci.19777

of interaction between infills and frames on the collapse performance of the non-ductile RC frame in 1920s. Mohammad et al. [17] analyzed three common structures: bare frame, uniformly infilled frame and partially infilled frame, with a prototype as three-story non-ductile concrete frame building that represents the Italian design practice of the 1970s. The results displayed the importance of correctly accounting for columns shear failure, the influence of inelastic shear law and different infills configurations.

Almost all of the aforementioned researches are aimed at ascertaining adverse effects of infills-frame interaction for non-ductile buildings without considering seismic design, while ignoring the effects for structures with sufficient seismic performance which constitute common building cases of the 1990s in most urban areas.

In fact, the infills also have a negative impact on the ductile RC frame [18]. Therefore, some scholars have realized that the seismic performance of such a structure with infills should be re-evaluated. Kareem and Güneyisi [19] studied the nonlinear static responses of four ductile RC frames with different infills configurations. However, the study failed to consider the shear failure risk of columns due to the plastic hinge assumption used in the numerical model.

On the other hand, static analysis is insufficient to investigate the seismic performance of structures on account of the correlation between seismic risk and structural period [20], which can be affected by infills. This means that although infills could improve the stiffness and strength of a structure when the interaction is insufficient to induce column shear failure, the damage probability of the structure may be not certainly reduced. Thus, it is beneficial to evaluate seismic probabilistic reliability of a structure by performance-based earthquake engineering (PBEE) framework with seismic risk and structural fragility considered.

The purpose of this paper is to reveal the impact of infills on the seismic resistant ductile RC frame by comprehensively evaluating the failure mode, dynamic response and seismic reliability of frames with different ductile level under the condition of considering different infills configurations. In consideration of the inventory of existing buildings, the low-rise frame was adopted as investigation object. The failure modes and damage states of different systems were obtained through nonlinear static analysis, and the fragility curves of each structure under various performance levels were obtained by IDA analysis. Then the seismic reliability is evaluated by calculating the exceedances probability with seismic risk and structural fragility took into account.

2 Case study configurations

A RC frame built in the late 1990s in southwest China was selected as the prototype which designed in accordance with China code 1989 for seismic design of building [21], considering live loads of 0.5 kN/m^2 on the roof and 2.5 kN/m^2 on normal floors, respectively. The slabs are made of reinforced concrete with a thickness of 100 mm. Hollow clay brick is selected for infills with 200 mm thickness. In particular, masonry infill strength (f_{me}) is 10.5 Mpa, cracking shear strength (τ_{cr}) is 0.49 Mpa, Young's modulus (E_w) 5270 Mpa and shear modulus (G_w) 2100 Mpa. The compressive strength of the concrete (f_c') is set to 20.75 MPa. The yield strength of steel bars (f_y) is 360 MPa. The elevation and section reinforcement information of the structure are displayed in Fig. 1.

According to different infills configurations, models can be divided into bare frame (BF), upper-infilled frame (UIF) and all-infilled frame (AIF) as shown in Fig. 2. Stirrup-reduction frames, named BFS, AIFS and UIFS, are created to simulate a medium-low ductility frame by ignoring stirrup encryption at the column end. All of these frames meet the requirements of "strong column - weak beam" and "strong shear - weak flexure".

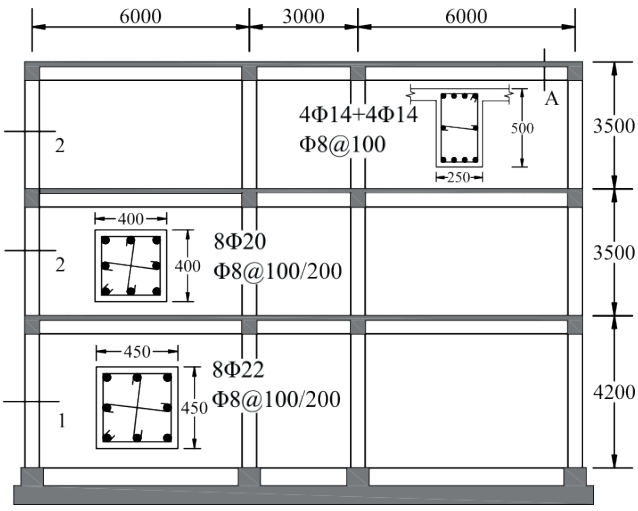

Fig. 1 Elevation and section information of the structure (Unit: mm)

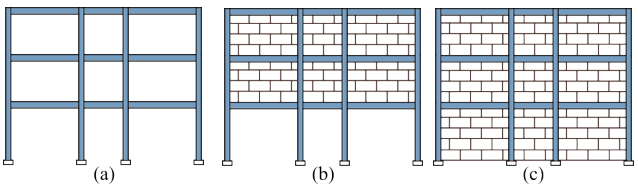

Fig. 2 Frames with various infills configurations: (a) BF, (b) UIF, (c) AIF

3 Nonlinear models and general assumptions

3.1 Frame modeling

In present study, fiber sections in OpenSEES are introduced to simulate beams and columns, as shown in Fig. 3. Steel reinforcement and concrete are modeled using Concrete02 and Steel02 materials, respectively. Force-beam-column element is adopted to model the beam and column, and disp-beam-column element is adopted to simulate the component of short column separated by the equivalent strut to obtain more accurate results. In addition, the beam section is modeled as T-shape to take into account the enhancement effect of slab. Giuffré-Menegotto-Pinto model [22] is adopted to define steel behavior while the Mander formulations [23] are employed to define the stress-strain relationships of constrained and unconstrained concrete.

The sliding behavior of reinforcement, the flexure behavior and the shear behavior of the column are coupled to each other at the element level through equilibrium and coordination conditions as shown in Fig. 3.

To consider the rotation displacement induced by strain penetration and bond slip of longitudinal reinforcement, a zero-length rotating spring with elastic properties is introduced in the model. The elastic stiffness of the spring is calculated through the theory introduced by Elwood and Eberhard [24].

The shear behavior of the column is modeled by adding a zero-length shear spring element which is connected in series with the rotational spring element. The stress-strain relationship is simulated by Ibarra-Medina-Krawinkler deterioration model (ModIMK) [25] as shown in Fig. 4(a).

In this study, a simple formula is employed to determine the initial elastic shear stiffness Ke:

$$K_e = \frac{5}{6}\frac{G \cdot A_g}{L} = \frac{E_c \cdot A_g}{3L}, \tag{1}$$

where, G the shear modulus of concrete; A_g the gross area of column section; L the length of the column section.

The shear strength V_n of the column is calculated according to ASCE/SEI 41-13[26] and the influence of axial load is ignored.

$$V_n = \frac{A_v f_{yt} d}{s} + \frac{0.5\sqrt{f_c'}}{a/d}\sqrt{1+\frac{P}{0.5\sqrt{f_c'}A_g}}\,0.8A_g, \tag{2}$$

where a/d the shear span ratio; A_v the total cross-sectional area of stirrup bars; f_{yt} yield strength of stirrup bars; d effective height of the section; s the center spacing of stirrup bars; P the axial load.

The plastic strain before the peak bearing capacity Δp and the ultimate strain after the peak bearing capacity Δpc can be calculated as follows [27]:

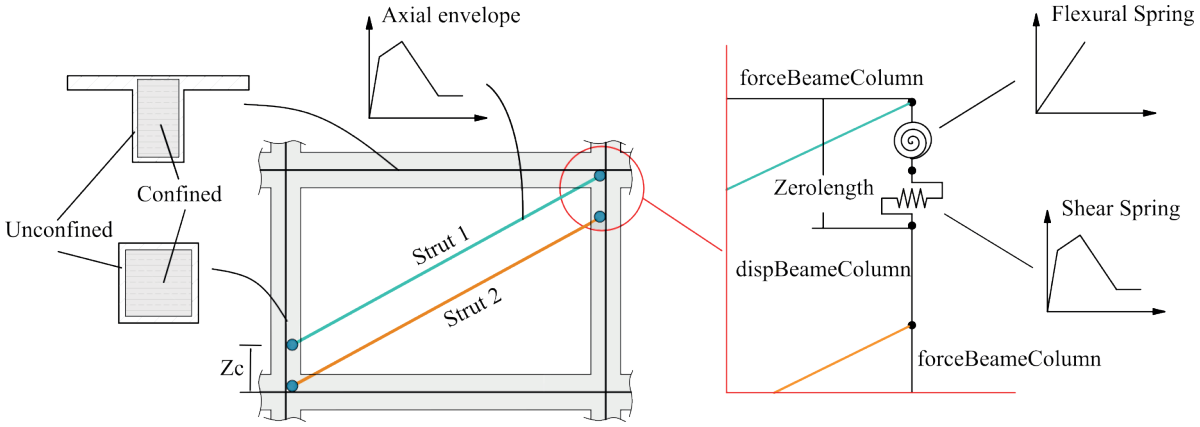

Fig. 3 Description of the numerical model

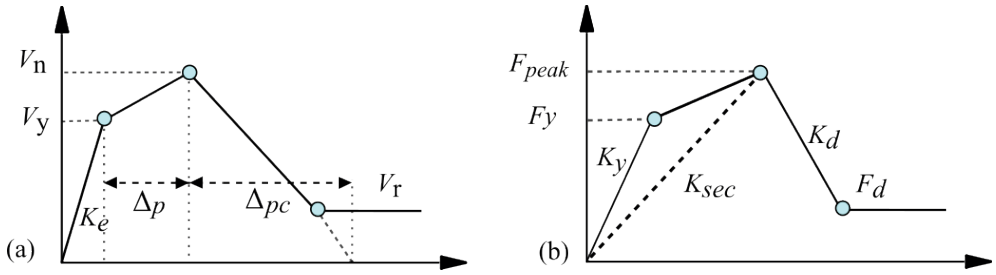

Fig. 4 Force-displacement envelope: (a) shear behavior of the column, (b) equivalent strut of infills

$$\Delta_p = 0.12 \cdot n^{-0.704} \cdot \left(\frac{a}{d}\right)^{1.653} \cdot \left(\frac{f_{yt} A_V}{f_c' A_g}\right)^{0.984}, \quad (3)$$

$$\Delta_{pc} = 0.167 \cdot n^{-0.839} \cdot \left(\frac{s}{d}\right)^{-0.033} \cdot \rho_t^{0.382}, \quad (4)$$

where n the axial pressure ratio and ρ_t the transverse reinforcement ratio.

The yield shear force V_y and residual shear strength V_r can be assumed as 75% and 20% of the peak shear strength V_n, respectively [28].

3.2 Modeling of infills

The infilled frame can be modeled separately, through nonlinear RC frame and macro modeling of masonry (double-strut). The nonlinearity of infills is obtained by assigning appropriate skeleton curves to the material of the structs. In this paper, the double-strut model [29] is adopted to simulate the infills. The assumption allows providing two parallel truss elements on the diagonals of each infills panel, with an eccentric distance (Z_c) from the frame joints, as shown in Fig. 3. The definition of eccentric distance is obtained from equivalent width bw and the angle between the strut and beam θ according to Eq. (5) proposed by Al-Chaar [30]:

$$Z_c = \frac{b_w}{2\cos\theta}. \quad (5)$$

The equivalent width (b_w) of the diagonal zone in the infills panel can be calculated through Eq. (6), which was also recommended by FEMA 356 [31].

$$b_w = d_w \cdot 0.175 h_w^{-0.4} \cdot \sqrt[4]{\left(\frac{E_w t_w \sin(2\theta)}{4EIh_w}\right)} \quad (6)$$

Where d_w, h_w, t_w the diagonal length, height and thickness of panel, respectively, E_w the Young's modulus of masonry wallboard, EI the flexural rigidity of concrete column.

In this paper, an improved mechanical model presented by De Risi et al. [32] was adopted, as exhibited in Fig. 4(b). Equivalent strut was modeled by the Truss element which not included geometric nonlinearities. The axial compression nonlinear characteristics were realized by the macro envelope of the uniaxial material to obtain the response of the infills. In this case, equivalent struts can simulate the yield or failure of the infills thus obtaining the affected response of the frame-infills system (e.g., increase and decrease in global strength).

The milestone points in Fig. 4(b) can be obtained by the Eqs. (7)–(13) [32]:

$$F_{peak} = \tau_{cr} A_w = \tau_{cr} L_w t_w, \quad (7)$$

$$F_y = 0.7 F_{peak}, \quad (8)$$

$$F_d = 0.05 F_{peak}, \quad (9)$$

$$K_{MS} = E_w t_w b_w / d_w, \quad (10)$$

$$K_y = 2.8 K_{MS}, \quad (11)$$

$$K_{sec} = 0.8 K_{MS}, \quad (12)$$

$$K_d = 0.1 K_{MS}, \quad (13)$$

Where, τ_{cr} the cracking shear strength of infills.

Pinching4 uniaxial material was employed to define the hysteresis behavior of equivalent struts, and the tensile envelope curve was assumption as near-zero values to realize the compression-only elements. The cyclic stiffness degradation parameters proposed by Kumar et al. [33] are adopted. Strength degradation parameter was set to 0.15. stiffness degradation parameter was set to 0.5. For pinching parameters, the value of 0.12 and 0.5 were adopted for strength and deformation in the present study to obtain appropriate calibrated results.

The proposed numerical model was calibrated and compared with an experimental result of infills frame from the research of Yuksel and Teymur [34] in Fig. 5.

It can be seen the stiffness and peak strength are underestimated by the FE model. However, the results are still acceptable due to the error within a small range.

4 Nonlinear static analyses

4.1 Damage criterion

The failure modes of six frame models with different configurations are realized by means of nonlinear static force pushover, respectively. As shown in Fig. 6, different damage

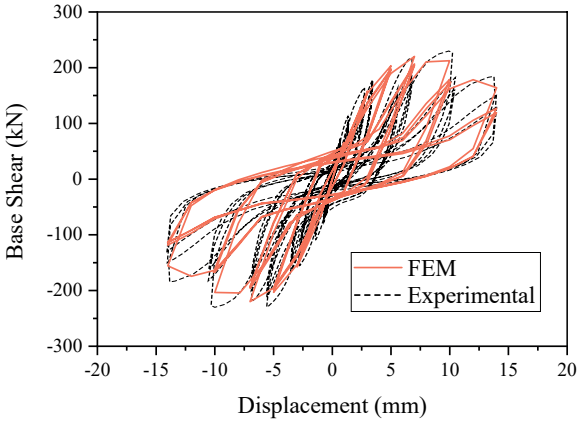

Fig. 5 The comparation between numerical and test result

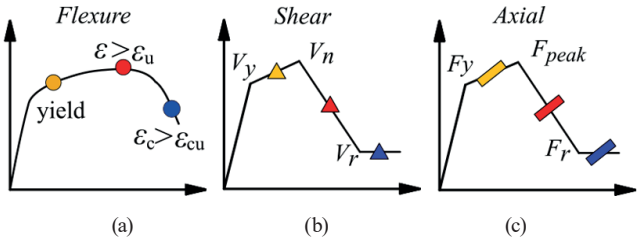

Fig. 6 Damage state of components: (a) Bending failure mode, (b) Shear failure mode, (c) Compression failure mode of equivalent strut

states including slight, moderate and serious damage of each component are defined for the sake of distinguishing the damage degree of the structure. For concrete beams and columns, the three flexure damage states (Fig. 6(a)) correspond to the yield of steel reinforcement, the state when the compressive strain of concrete cover plate reaches ultimate value ε_u = 0.0033 according to GB 50010 [35], and compressive strain of core concrete reaches ultimate value ε_{cu}, which is calculated by the following formula :

$$\varepsilon_{cu} = (2.34 + 2.49\lambda_v^{0.73})(1 + 3.5\lambda_v)\varepsilon_{c0}\,, \tag{14}$$

where ε_{c0} the peak strain of plain concrete, set to be 0.002; λ_v the volume transverse reinforcement ratio.

The shear damage states of concrete members are demarcated according to different stages on the envelope curve. Slight, moderate and serious shear damage states correspond to the yield stage on the envelope curve, the post-peak stage, and the residual stage, respectively (Fig. 6(b)). Similarly, three damage states of infills are defined as shown in Fig. 6(c).

The performance level represents the performance of a global structure, and can be quantified by inter-story drift ratio (IDR). The three standard PBEE performance levels, namely Immediate Occupancy (IO), Life Safety (LS) and Collapse Prevention (CP), as defined by FEMA356 [31], are considered in the assessment framework, with corresponding IDRs of 1%, 2% and 4%, respectively.

4.2 Numerical results of static analyses

The nonlinear static analysis results are shown in Fig. 7. The cutoff point of the structural capability curve conforms to one of the following characteristics: (a). the maximum IDR exceeds 4%; (b). the column suffers severe shear failure.

Fig. 8 shows damage patterns of the six structures at various performance levels. The corresponding base shear and roof drift are shown in Table 1. It should be pointed out that reference IDR value recommended by FEMA is not adopted for performance level of structure with severe shear damage and brittle failure. In another way, the performance level is designated by considering the damage of vertical components, and the maximum IDR is recalculated.

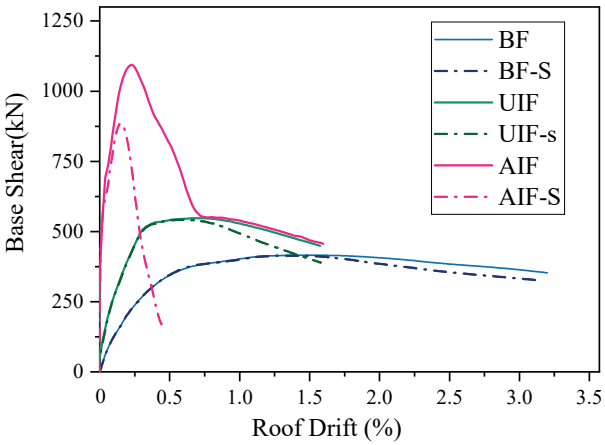

Fig. 7 Pushover curves of different frame

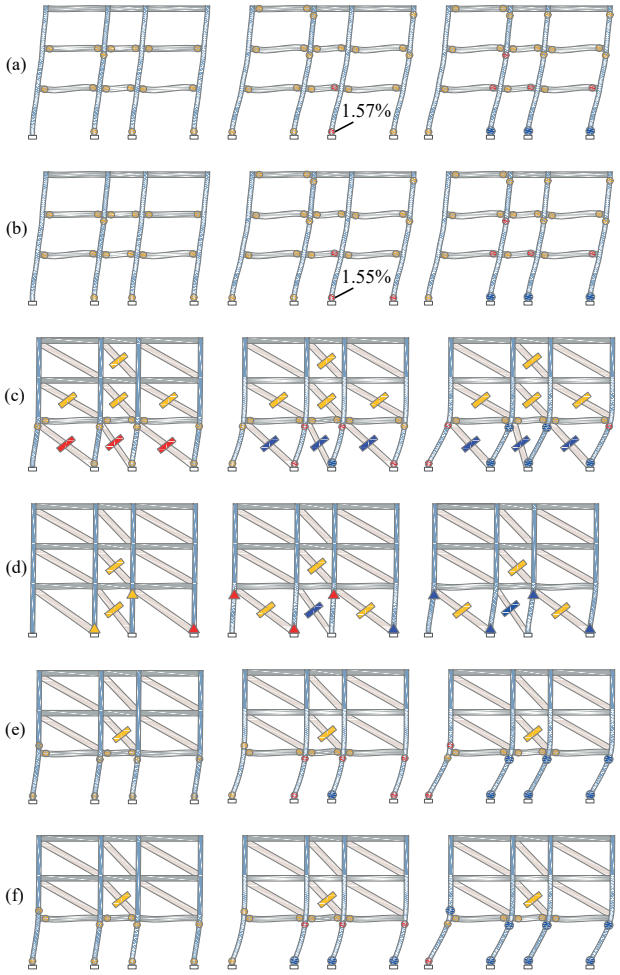

Fig. 8 Damage patterns of structure variants: (a) BF, (b) BFS, (c) UIF, (d) UIFS, (e) AIF, (f) AIFS

Table 1 Performance Level and failure modes of different frames

	Parameters	Performance Level			Failure mode
		IO	*LS*	*CP*	
BF	V (kN)	389.10	415.15	352.35	Flexure
	D_R (%)	0.82	1.63	3.20	
BFS	V (kN)	388.74	408.87	326.55	Flexure
	D_R (%)	0.82	1.63	3.13	
UIF	V (kN)	534.42	545.19	450.63	Soft story
	D_R (%)	0.43	0.81	1.57	
UIFS	V (kN)	530.88	528.09	391.03	Soft story
	D_R (%)	0.42	0.81	1.57	
AIF	V (kN)	931.95	551.61	457.8	Soft story
	D_R (%)	0.45	0.83	1.59	
AIFS	V (kN)	772.54	243.25	158.79	Shear
	D_R (%)	0.08	0.17	0.43	
	IDR_{max} (%)	0.11	0.24	1.10	

Note: Where V the base shear of the building; D_R the top drift ratio; IDR_{max} the maximum of interlayer drift ratios for all three floors.

4.2.1 BF

Uniform inter-story deformation occurs in BF (Fig. 8(a)), allowing all story to dissipate energy. The reinforcement at beam end yields first, hence plastic hinges appear at the beam earlier than column which allows a relaxation of the constraint on column end and avoids severe damage of the column as a result. Damage pattern shows a typical failure mechanism of "strong-columns and weak-beams". At IO performance level, slight flexure damages occur at a part of beam ends and column bottoms in the first story. At SL performance level, plastic hinges appear on the top floor of BF. Moderate flexure damage is derived at the end of the beam in the central bay and the bottom of the column on the first floor. The structure still has an adequate safety margin. At CP performance level, more than 50% of the beam ends on the first floor suffer moderate flexure damage, and the core concrete of the bottom column is crushed, causing severe flexure damage. On the whole, structural components suffer flexure failure that develops orderly in each story, which leads to a ductile failure mode.

4.2.2 BFS

Similar to BF, flexure failure in BFS occurs prior to shear failure Fig. 8(b)) despite the fact that shear strength is decreased owing to increase in distance of transverse reinforcement. The difference is that the damage of the bottom column in BFS at SL level is more serious than that in BF. Actually, moderate flexure damage first occurred when IDR = 1.57% (corresponding Roof Drift is 1.25%) in BF, and the same failure occurs when IDR = 1.55% (corresponding Roof Drift is 1.23%) in BFS. After that, performance curves of BF and BFS begin to show significant differences (it can be seen from Fig. 7 that the base shear of BFS is continuously lower than that of BF after Roof Drift = 1.5%). This discrepancy could be attributed to the constraint ability of transverse reinforcement. In stirrup-reduction frames, the constraint effect of transverse reinforcement on core concrete is certainly slighter than normal frame, which leads to the fact that the core concrete of BFS will be crushed with stress decreased earlier than that of BF.

4.2.3 UIF

Damage patterns of UIF show a soft-story mechanism. The stiffness of upper stories in the structure is greatly strengthened by infills, thus the deformation of the structure is mainly concentrated on the first story with low stiffness. At IO performance level, the infills in the central bay on the second floor are slightly damaged, with reinforcement of the beam and column ends on the first floor yield. Different from BF, the global deformation is mainly caused through the rotation of the column, resulting in more plastic hinge appearing at the column end of UIF frame. The reason is that infills on the second floor has a constraint effect on the frame joints, which reduce the chord rotation of the beam end and the column bottom on the second floor, and indirectly increase the stiffness of the beam, hence change the "strong-column and weak-beam" mechanism. Simultaneously, as the structural deformation is mainly controlled by the frame column, the initial stiffness and peak base shear of UIF are higher than BF (Fig. 7). At SL performance level, deformation continues to develop on the ground floor, while upper floors are still not significantly deformed. At CP level, serious flexure damage occurred at both ends of the bottom column while the frame beam attached to the column suffered only slight damage. The analytical results also indicate that the damage degree of bottom column in UIF is significantly higher than that in BF under the same IDR value, which leads to a more obvious decline of UIF capacity curve in the latter loading period.

4.2.4 UIFS

Fig. 8(d) demonstrates that UIFS also has the failure mechanism of the soft-story. The pushover curve of UIFS is indistinguishable with that of UIF at the beginning of loading. Due to the reduction constraint effect of stirrup, serious flexure damage at the end column of UIFS occurs earlier than that of UIF (for example, there are

more locations in serious flexure damage in UIFS at IDR = 2%), which is in accord with the dissimilarity Between BF and BFS. As a result, the base shear of UIFS is lower than that of UIF in the late loading stage. Compared with BF and BFS, the deviation is more obvious due to more severe damage of the bottom column.

4.2.5 AIF

Fig. 8(e) shows the soft-story mechanism in UIFS. At IO performance level, infills on the first floor was seriously damaged, while slightly damage states occur in the second floor and the central bay of the third floor. Particularly, early failure and strength decline of the first story infills induce the significant discrepancy of drift between the first floor and upper floors, which lead to the soft-story mechanism. And due to the constraint effect of infills to frame joints, the damage and chord rotation mainly occur in columns. At SL performance level, the first story infills are completely destroyed, while the damage on the upper floors is not further developed. The deformation of the structure depends on the first story, and the core concrete is crushed at the bottom of the column. At CP performance level, the damage continued to develop in the first story, and several severe flexure failure modes occur in the bottom columns.

4.2.6 AIFS

Shear failure occurs in AIFS, and the IDR value corresponding to the state of complete failure at all the columns is 1.24% (corresponding Roof Drift is 0.49%). Therefore, every performance level is re-quantified. IO performance level is set to IDR = 0.11%. At this state, the first slight shear damage occurs in a column, and infills in the central bay of the 1st and 2nd floors is slightly damaged. When IDR = 0.24%, the first moderate shear damage occurs at the bottom of the border column, this state is defined as SL performance level. CP performance level is set to IDR = 1.1%, with complete shear failure occurring at the bottom of the border column, and the shear force at the end of other columns has reached the value of shear capacity. Infills in border bays of the first floor enters the yield stage and internal force of which gradually decreases, with the shear demand in the column contacted surpassing the shear capacity. Nevertheless, the shear force of the column in the central bay has not reached the shear yield value until infills completely collapse due to the lower strength produced by smaller geometry size of the infills. As a whole, the global capacity of AIFS is determined only by the shear capacity of the column. Therefore, the peak strength of AIFS in Fig. 7 is substantially lower than that of AIF, whose strength is provided by frame and padding. This implies that for concrete frames with low stirrup ratio, the impact of infills on the frame is prominent, and strong infills may lead to brittle shear failure in the column.

Fig. 9 shows the maximum shear demand (MSD) and shear capacity ratio (SCR) of the bottom column in each frame. Except for the All-infilled Frames, the MSDs of the bottom column in other frames with different stirrup configurations are basically equal. However, due to the reduction of column shear capacity in the frames with low stirrup ratio, their SCRs are higher compared with normal stirrup frames.

It can also be observed from the figure that the MSDs of UIF and UIFS are higher than those of BF and BFs, and the SCR of UIFS reaches 77% even no infill wall is equipped in the first story. This can be ascribed to the failure mode of the soft-story mechanism, which conspicuously amplifies the chord rotation demand of the first floor column and increases the shear demand consequently. For All-infilled Frames, even with dense hooped reinforcement in the column, the SCRs still exceeds 90%. Considering the uncertainty of infills material and frame mechanical property in practical engineering, structures of this type have a high risk of shear failure.

5 Nonlinear dynamic analysis and probabilistic seismic reliability evaluation

5.1 Ground motions and dynamic properties of the structures

A set of 20 natural accelerograms are chosen from the PEER database, and satisfy the demand of spectrum coordination with the design spectrum in GB50011 [36] with 457 years return period. The selected Ground Motion (GM) records

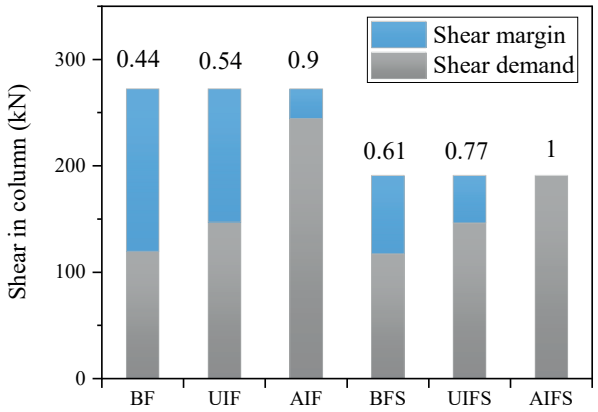

Fig. 9 Maximum shear demand and shear capacity ratio of bottom column

are shown in Fig. 10, including the average spectrum and the site target spectrum (475 years return period) in GB50011 [36]. To perform incremental dynamic analysis, the selected accelerograms are scaled to a value of $S_a(T_1) = 0.1$ g in correspondence to the fundamental period T1 for every structure. Eigenvalue analyses are carried out with the fundamental periods listed in Table 2, which shows that the reduction of stirrup has little effect on the dynamic characteristics of structures. However, the dynamic characteristics are dramatically affected due to the infills configuration, with the periods of UIF and AIF shorten by about 23% and 70% than BF.

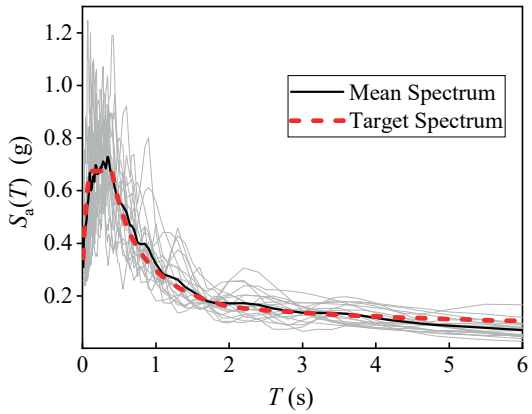

Fig. 10 The selected Ground Motion (GM) records

Table 2 Main dynamic properties (unit: s)

	BF	BF-S	UIF	UIF-S	AIF	AIF-S
T1	0.483	0.484	0.372	0.372	0.147	0.147

5.2 Numerical results of Incremental dynamic analysis

IDA results of the six frame models are reported in Fig. 11. The IDA curve features of BF and BFS (Fig. 11(a) and Fig. 11(b)), UIF and UIFS (Fig. 11(c) and Fig. 11(d)) are basically similar, while the curve of AIF (Fig. 11e) is significantly different from that of AIFS (Fig. 11(f)). At a very small IDR value (less than 1%), the IDA curve of AIF (S) has a large slope owing to additional stiffness provided by infills. With the increase of IDR value, the slope of the curve suddenly decreases, which means that the structure is destroyed on the spur of the moment.

For AIF, this abrupt change is caused by the failure of infills, and the subsequent curve still has a certain slope, which indicates that the frame column can continue to provide support against the load. While this change in AIFS can be regarded as the consequences of the excessive shear demand generated by the interaction between infills and columns. The seismic capacity of the structure decreases sharply and IDA curve flattens out with columns failing by shear. Moreover, aforementioned mutation occurred earlier in AIFS than AIF with remarkably smaller S_a value.

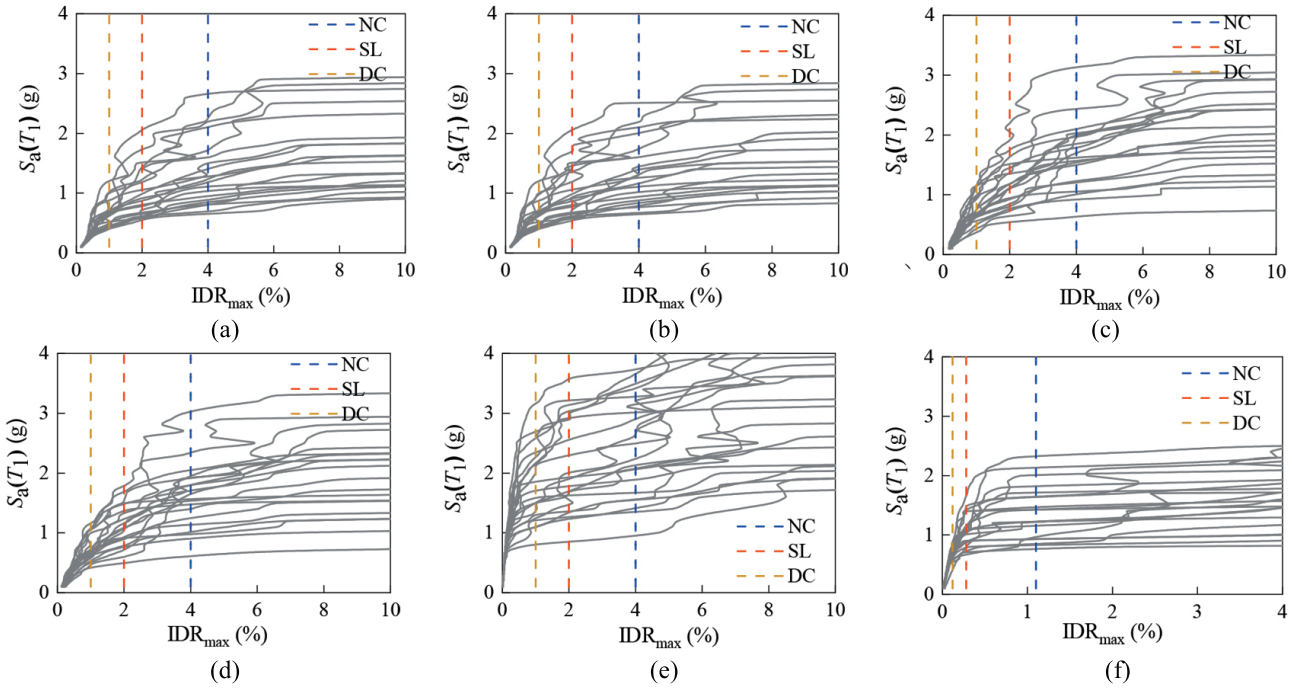

Fig. 11 IDA curve with performance levels for: (a) BF, (b) BFS, (c) UIF, (d) UIFS, (e) AIF, (f) AIFS

5.3 Fragility assessment

The fragility curves of the structure can be derived from the results of IDA [37] using the following analytical expression:

$$P[C \le D|IM = x] = \Phi\left(\frac{\ln(x) - \mu_{\ln x}}{\sigma_{\ln x}}\right), \quad (15)$$

where $P[C \le D|IM = x]$ the probability that a ground motion with intensity measure $IM = x$ will cause the achievement of a performance level; Φ is the standard cumulative distribution function; μ_{lnx} is the mean value and σ_{lnx} is the standard deviation of the natural logarithms of the distribution of x. The fragility curves of different performance level of each structure are shown in Fig. 12.

The fragility curves of BF and BFS of the three performance levels almost coincide (Fig. 12(a)), which means that the two structures have roughly the same seismic performance, which is in accord with the results on UIF and UIFS (Fig. 12(b)). On the contrary, the fragility curves of AIFS and AIF are enormously deviating (Fig. 12(c)). The former shows obvious early failure characteristic, and the curve corresponding to any limit state is far to the left of the curve of AIF. It needs to be mentioned that, since the IDA curve of AIFS tends to be flat after IDR = 1%, the fragility curve corresponding to SL or CP limit state of AIFS framework will not be considerably divergent from the curve in Fig. 12(c) even if the drift ratio recommended by the code is adopted as the limit states measurement.

On the other hand, compared with other frames, the curves of different limit states of AIF are closer, which illuminates the structure has contiguous IMs for different performance levels. In other words, under a certain ground motion intensity, the probability of the structure reaching different limit states is close, which means that the structure is more likely to transition from the former limit state to the latter one. This can be explained as follows: the infills which will be destroyed easily can participate in the earthquake resistance and absorb energy of the ground motion through self-damage. As IM grows, the soft-story mechanism caused by infills failure leads to rapid development of structural damage.

There is no obvious difference between BF and UIF, by comparing Fig. 12(a) and Fig. 12(b). However, it should be pointed out that the damage patterns diagram (Fig. 8) in Section 4.2 shows significantly more serious structural damage of UIF than BF (the damage of the former is mainly in the column) under the same limit state.

AIF showed a larger IM corresponded to the same performance level than UIF, by Comparing Fig. 12(b) and Fig. 12(c), despite of the same failure model of soft-story. This can be attributed to the large initial stiffness of the AIF, which needs greater force to induce the limit state. After the failure of infills, the period of structure changes and avoids the amplitude modulated period T1, which leads to a smaller response of the structure under the same parameter $IM = S_a(T_1)$.

However, it is not reasonable to compare the seismic performance of different structures by directly comparing the fragility curves. In fact, the intensity measures and seismic hazard curves are related to the vibration period of the structures. In this view, reliability assessment is introduced to compare the performance of different structures.

5.4 Seismic hazard and reliability evaluation

The performance-based seismic engineering (PBEE) framework allows considering the major earthquakes as a uniform Poisson process (HPP). Under this assumption, the event process leading to structure failure can also be represented by HPP, and then the occurrence-probability of a specific structure reaching a certain limit state within a reference time period can be obtained through the coupling of seismic hazard curve and fragility curve of the structure.

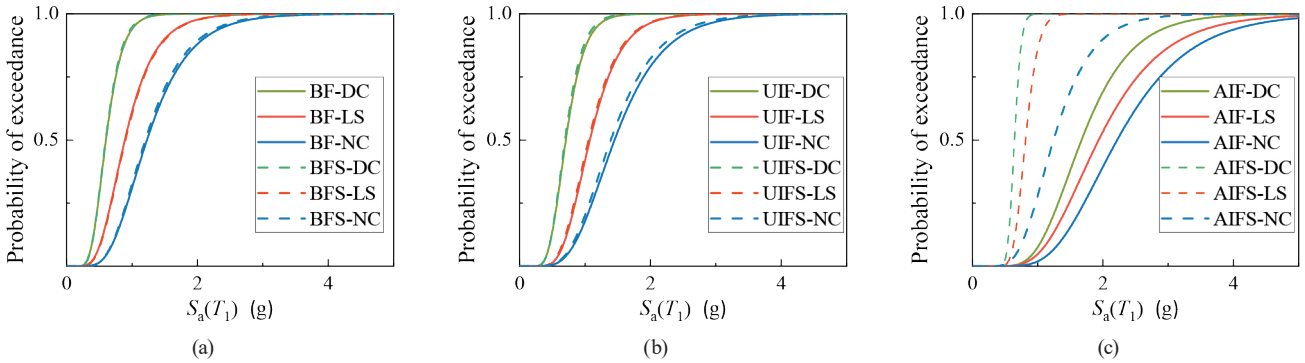

Fig. 12 Analytical fragility curves for: (a) bare frames, (b) upper-infilled frames, (c) all-infilled frames

Seismic risk is a function that describes the annual rate of exceeding, represents seismic activity at a particular site. The seismic risk curve can be approximately described by the following formula [38]:

$$\lambda(x) = k_0 x^{-k}, \tag{16}$$

where k_0 and k the shape coefficients of the curve, can be derived by interpolating design response spectrum.

Then the probability of exceeding an $IM = S_a(T)$ in a specific site in the reference period (N years) can be derived as:

$$H[IM \geq x, T, N] = H(x) = 1 - e^{-N\lambda(x)} k_0(x)^{-k}. \tag{17}$$

Fig. 13 shows the hazard curves of the considered structures, represent the probability that the ground motion intensity index $IM = S_a(T_1)$ exceeds a specific value within 50 years. The occurrence-probability of a specific structure reaching a certain limit state can be expressed as:

$$P_f = \int_0^{\infty} P[C \leq D | IM = x] \cdot h[\mathrm{IM} \geq x, T, N] dx, \tag{18}$$

where $h[IM \geq x, T, M]$ is the probability density function of $IM = S_a(T)$, and can be derived from the cumulative distribution function $H(x)$:

$$h[IM \geq x, T, N] = h(x) = d[1 - H(x)] / dx. \tag{19}$$

In particular, P_f is positively correlated with the intersection area of risk probability density function curve $h(x)$ and fragility curve $P(x)$. Fig. 14 highlights the different amplitudes of the intersection areas between hazard and fragility curves. It can be seen that a lower fragility value not always means a lower failure probability as a result of the difference of earthquake risk curves.

Probabilities of occurrence (P_f) calculated from Eq. (11) are summarized as bar charts in Fig. 15. Similar to the previous analysis conclusion, there is little disparity in seismic reliability between BF and BFS with different column stirrup ratios, as well as UIF and UIFS. The occurrence probabilities of UIF are relatively high among the systems with different infills configurations and normal densification stirrup arrangement due to the soft-story mechanism. Because of the uniform IDR used in the calculation, exceedance probabilities of SL limit state of UIF is close to BF. However, as described in Section 5.3, UIF has more serious structural damage. In addition, severe damage on the UIF has occurred in SL state, indicating that there is a higher risk of structural collapse under the same IDR.

The occurrence probability of AIF at IO level is lower than that of other frames, which indicates that the infills play a role in providing stiffness and absorbing seismic energy through damage, significantly increases the ground motion intensity $S_a = x$ required by the frame to enter the IO state as a result. However, the structural damage developed rapidly after the failure of infills, resulting in a high P_f of 0.77% at the CP level which means that the collapse

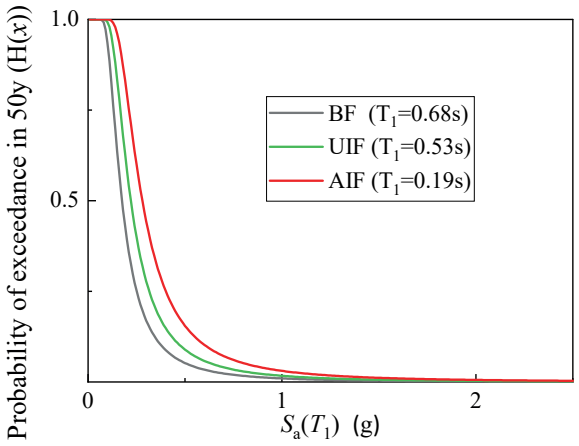

Fig. 13 Hazard curves for different structures

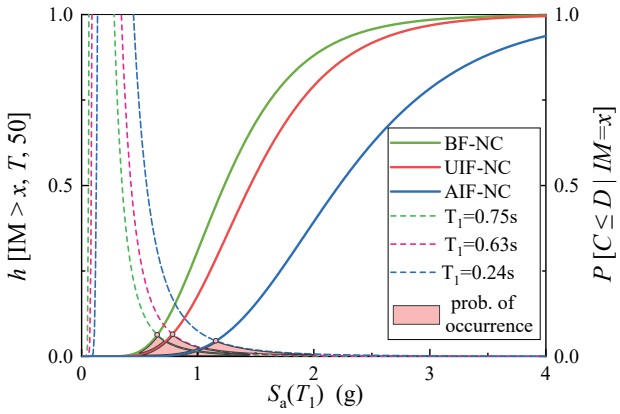

Fig. 14 The intersection areas of fragility curves and hazard curves

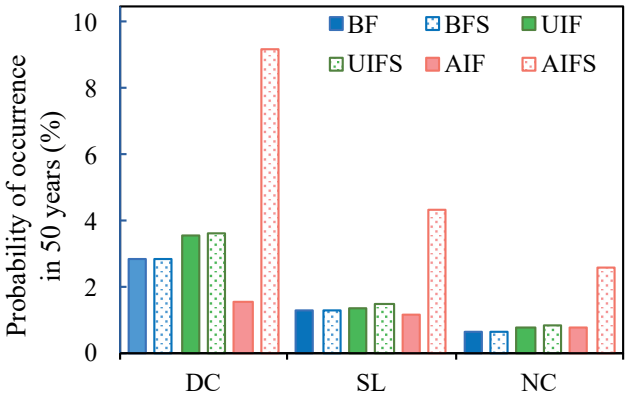

Fig. 15 Probabilities of occurrence in 50 years

probability is higher than BF and UIF. This result is significantly different from that of the fragility curve in Fig. 12, which shows that AIF has a prominent better performance. The reason is that the vibration period of AIF is obviously shorter which provides a significantly higher hazard and ultimately leads to a high occurrence probability cacu-lated by Eq. (11). Although infills can provide rigidity and energy dissipation capacity, it will increase seismic demand at the same time. Considering the early failure of infills due to insufficient ductility, the response of such structures to strong earthquakes is often difficult to predict.

The occurrence probability AIFS is much higher than other frames for any performance level. This is first due to the same high seismic hazard level produced by the short periods as in AIF. Secondly, the shear failure in columns caused by infills-column interaction exhibited the infills in AIFS played a negative role rather than provided effective seismic resistance as in AIF.

6 Conclusions

The proposed research presents an evaluation for existing ductile RC frame structures with the consideration of infills-frame interaction. The failure modes and seismic reliability of the structures was investigated. Within the scope of the present investigation, main conclusions can be drawn as follows:

a) The infills arrangement can significantly affect the seismic response of structures. The exceedance probabilities of UIF are higher than that of BF owning to soft-story damage patterns.

b) For the structures analyzed in the work, a uniform infills distribution cannot guarantee the requisite seismic performance of the structure. IDA curves and fragility curves show that subsequent damage in AIF develops more rapidly than UIF after the failure of infills. The collapse probability of AIF is higher than BF and UIF owning to greater seismic action caused by shorter period and the rapid damage progression in infills. This means that even if the shear resistance of the column is sufficient to resist the infills-column interaction, it is not appropriate to regard the design result of infills as conservative.

c) AIFS shows a brittle shear failure mode, though the transverse ratio meets the calculation requirements of "strong shear and weak bend" in the code. Therefore, special attention needs to be paid to the impact of infills - column interactions of these types of building, even for ductile structures.

d) It is worth mentioning that since the conclusion is based on the structures in the present research, future studies extended could be carried out on other types of infill blocks and high-rise structures to extend the conclusions.

References

[1] Yu, X., Li, Y., Lu, D., Jia, M., Fan, F. "Fragility-based probabilistic seismic safety assessment of RC frame structures with infilled masonry walls", China Civil Engineering Journal, 47(S2), pp. 260–265, 2014.
https://doi.org/10.15951/j.tmgcxb.2014.s2.042

[2] Vicente, R. S., Rodrigues, H., Varum, H., Costa, A., Raimundo, J. A., Da Silva, M. "Performance of masonry enclosure walls: lessons learned from recent earthquakes", Earthquake Engineering and Engineering Vibration, 11, pp. 23–34, 2012.
https://doi.org/10.1007/s11803-012-0095-3

[3] Negro, P., Colombo, A. "Irregularities induced by nonstructural masonry panels in framed buildings", Engineering Structures, 19(7), pp. 576–585, 1997.
https://doi.org/10.1016/s0141-0296(96)00115-0

[4] Haldar, P., Singh, Y., Paul, D. K. "Identification of seismic failure modes of URM infilled RC frame buildings", Engineering Failure Analysis, 33, pp. 97–118, 2013.
https://doi.org/10.1016/j.engfailanal.2013.04.017

[5] De Luca, F., Verderame, G. M., Gómez-Martínez, F., Pérez-García, A. "The structural role played by masonry infills on RC building performances after the 2011 Lorca, Spain, earthquake", Bulletin of Earthquake Engineering, 12, pp. 1999–2026, 2014.
https://doi.org/10.1007/s10518-013-9500-1

[6] Haris, I., Hortobágyi, Z. "Comparison of experimental and analytical results on masonry infilled RC frames for monotonic increasing lateral load", Periodica Polytechnica Civil Engineering, 56(2), pp. 185–196, 2012.
https://doi.org/10.3311/pp.ci.2012-2.05

[7] Haris, I., Hortobágyi, Z. "Comparison of Experimental and Analytical Results on Masonry Infilled RC Frames for Cyclic Lateral Load", Periodica Polytechnica Civil Engineering, 59(2), pp. 193–208, 2015.
https://doi.org/10.3311/PPci.8099

[8] Asteris, P. G., Cotsovos, D. M. "Numerical Investigation of the Effect of Infill Walls on the StructuralResponse of RC Frames", The Open Construction and Building Technology Journal, 16, pp. 164–181, 2012.
https://doi.org/10.2174/1874836801206010164

[9] Haris, I., Hortobágyi, Z. "Different FEM models of reinforced concrete frames stiffened by infill masonry for lateral loads", Periodica Polytechnica Civil Engineering, 56(1), pp. 25–34, 2012.
https://doi.org/10.3311/pp.ci.2012-1.03

[10] Chrysostomou, C. Z., Gergely, P., Abel, J. F. "A Six-Strut Model for Nonlinear Dynamic Analysis of Steel Infilled Frames", International Journal of Structural Stability and Dynamics, 2, pp. 335–353, 2002.
https://doi.org/10.1142/S0219455402000567

[11] Kong, J., Zhai, C., Wang, X. "In-Plane Behavior of Masonry Infill Wall Considering Out-of-Plane Loading", Periodica Polytechnica Civil Engineering, 60(2), pp. 217–221, 2016. https://doi.org/10.3311/PPci.7867

[12] Al Hanoun, M. H., Abrahamczyk, L., Schwarz, J. "Macromodeling of in- and out-of-plane behavior of unreinforced masonry infill walls", Bulletin of Earthquake Engineering, 17, pp. 519–535, 2019. https://doi.org/10.1007/s10518-018-0458-x

[13] Mazza, F. "In-plane–out-of-plane non-linear model of masonry infills in the seismic analysis of r.c.-framed buildings", Earthquake Engineering and Structural Dynamics, 48(4), pp. 432–453, 2019. https://doi.org/10.1002/eqe.3143

[14] Uva, G., Raffaele, D., Porco, F., Fiore, A. "On the role of equivalent strut models in the seismic assessment of infilled RC buildings", Engineering Structures, 42, pp. 83–94, 2012. https://doi.org/10.1016/j.engstruct.2012.04.005

[15] Celarec, D., Dolšek, M. "Practice-oriented probabilistic seismic performance assessment of infilled frames with consideration of shear failure of columns", Earthquake Engineering and Structural Dynamics, 42(9), pp. 1339–1360, 2013. https://doi.org/10.1002/eqe.2275

[16] Burton, H., Deierlein, G. "Simulation of Seismic Collapse in Nonductile Reinforced Concrete Frame Buildings with Masonry Infills", Journal of Structural Engineering, 140(8), Article number: A4014016, 2013. https://doi.org/10.1061/(ASCE)ST.1943-541X.0000921

[17] Mohammad, A. F., Faggella, M., Gigliotti, R., Spacone, E. "Seismic performance of older R/C frame structures accounting for infills-induced shear failure of columns", Engineering Structures, 122, pp. 1–13, 2016. https://doi.org/10.1016/j.engstruct.2016.05.010

[18] Basha, S. H., Kaushik, H. B. "Behavior and failure mechanisms of masonry-infilled RC frames (in low-rise buildings) subject to lateral loading", Engineering Structures, 111, pp. 233–245, 2016. https://doi.org/10.1016/j.engstruct.2015.12.034

[19] Kareem, K. M., Güneyisi, E. M. "Effect of Masonry Infill Wall Configuration and Modelling Approach on the Behaviour of RC Frame Structures", Arabian Journal for Science and Engineering, 44, pp. 4309–4324, 2019. https://doi.org/10.1007/s13369-018-3389-6

[20] Ahmadi, M., Naderpour, H., Kheyroddin, A., Gandomi, A. H. "Seismic Failure Probability and Vulnerability Assessment of Steel-Concrete Composite Structures", Periodica Polytechnica Civil Engineering, 61(4), pp. 939–950, 2017. https://doi.org/10.3311/PPci.10548

[21] National Standard of People's Republic of China "GB50011-1989 Code for seismic design of buildings", Ministry of Construction of the People's Republic of China, Beijing, China, 1989.

[22] Comité Euro-International du Béton "RC elements under cyclic loading: state of the art report", Thomas Telford, New York, NY, USA, 1996. [online] Available at: https://www.icevirtuallibrary.com/isbn/9780727739780

[23] Mander, J. A. B., Priestley, M. J. N. "Theoretical Stress-Strain Model for Confined Concrete", Journal of Structural Engineering, 114(8), pp. 1804–1826, 1988. https://doi.org/10.1061/(ASCE)0733-9445(1988)114:8(1804)

[24] Elwood, K. J., Eberhard, M. O. "Effective Stiffness of Reinforced Concrete Columns", ACI Structural Journal, 106(4), pp. 476–484, 2009. https://doi.org/10.14359/56613

[25] Ibarra, L. F., Medina, R. A., Krawinkler, H. "Hysteretic models that incorporate strength and stiffness deterioration", Earthquake Engineering and Structural Dynamics, 34(12), pp. 1489–1511, 2005. https://doi.org/10.1002/eqe.495

[26] ASCE "ASCE/SEI 41-13 Seismic evaluation and retrofit of existing buildings", American Society of Civil Engineers, Reston, VA, USA, 2014. https://doi.org/10.1061/9780784412855

[27] Xu, J.-G., Feng, D.-C., Wu, G, Cotsovos, D. M., Lu, Y. "Analytical modeling of corroded RC columns considering flexure-shear interaction for seismic performance assessment", Bulletin of Earthquake Engineering, 18, pp. 2165–2190, 2020. https://doi.org/10.1007/s10518-019-00770-6

[28] Jeon, J.-S., Lowes, L. N., DesRoches, R., Brilakis, I. "Fragility curves for non-ductile reinforced concrete frames that exhibit different component response mechanisms", Engineering Structures, 85, pp. 127–143, 2015. https://doi.org/10.1016/j.engstruct.2014.12.009

[29] Crisafulli, F. J. "Seismic Behaviour of Reinforced Concrete Structures with Masonry Infills", PhD Thesis, University of Canterbury, 1997. https://doi.org/10.26021/1979

[30] Al-Chaar G. "Evaluating strength and stiffness of unreinforced masonry infill structures", US Army Corps of Engineers, US Army Corps of Engineers, Engineer Research and Development Centre, Vicksburg, MS, USA, Rep. ERDC/CERL TR-02-1, 2002. [online] Available at: https://www.researchgate.net/publication/235149444

[31] FEMA356 "Prestandard and commentary for the seismic rehabilitation of building", Federal Emergency Management Agency, Washington, DC, USA, 2000. [online] Available at: https://www.nehrp.gov/pdf/fema356.pdf

[32] De Risi, M. T., Del Gaudio, C., Ricci, P., Verderame, G. M. "In-plane behaviour and damage assessment of masonry infills with hollow clay bricks in RC frames", Engineering Structures, 168, pp. 257–275, 2018. https://doi.org/10.1016/j.engstruct.2018.04.065

[33] Kumar, M., Rai, D. C., Jain, S. K. "Ductility reduction factors for masonry-infilled reinforced concrete frames", Earthquake Spectra, 31(1), pp. 339–365, 2015. https://doi.org/10.1193/110512EQS322M

[34] Yuksel, E., Teymur, P. "Earthquake performance improvement of low rise RC buildings using high strength clay brick walls", Bulletin of Earthquake Engineering, 9, pp. 1157–1181, 2011. https://doi.org/10.1007/s10518-010-9242-2

[35] National Standard of People's Republic of China "GB 50010-2010 Code for seismic design of concrete structures", Ministry of Construction of the People's Republic of , Beijing, China, 2015.

[36] National Standard of People's Republic of China "GB50011-2010 Code for seismic design of buildings", Ministry of Construction of the People's Republic of , Beijing, China, 2016.

[37] Baker, J. W. "Efficient Analytical Fragility Function Fitting Using Dynamic Structural Analysis", Earthquake Spectra, 31(1), pp. 579–599, 2015.
https://doi.org/10.1193/021113EQS025M

[38] Cornell, C. A., Jalayer, F., Hamburger, R. O., Foutch, D. A. "Probabilistic Basis for 2000 SAC Federal Emergency Management Agency Steel Moment Frame Guidelines", Journal of Structural Engineering, 128(4), pp. 526-533, 2002.
https://doi.org/10.1061/(ASCE)0733-9445(2002)128:4(526)